



PCCP

Thermodynamics of the S2-to-S3 State Transition of the Oxygen-Evolving Complex of Photosystem II

Journal:	<i>Physical Chemistry Chemical Physics</i>
Manuscript ID	CP-ART-04-2019-002308.R1
Article Type:	Paper
Date Submitted by the Author:	17-Jul-2019
Complete List of Authors:	Amin, Muhamed; Center for Free Electron Laser Science, ; Rijksuniversiteit Groningen Biomolecular Sciences and Biotechnology Institute, Matta, Divya; City College of the City University of New York Yang, Ke; Yale University, Chemistry Wang, Jimin; Yale University, Chemistry Mohamed, Zainab; Zewail City of Science and Technology Brudvig, Gary; Yale University-Chemistry, Gunner, M; City College of New York Batista, Victor; Yale University, Chemistry

SCHOLARONE™
Manuscripts

Thermodynamics of the S₂-to-S₃ State Transition of the Oxygen-Evolving Complex of Photosystem II

Muhamed Amin^{1,2,3*}, Divya Kaur^{4,5}, Ke R. Yang⁶, Jimin Wang⁷, Zainab Mohamed⁸, Gary W. Brudvig⁶, M.R. Gunner^{4,5} and Victor Batista⁶

¹ Center for Free-Electron Laser Science, Deutsches Elektronen-Synchrotron DESY, Notkestrasse 85, 22607 Hamburg, Germany

² Physics Department, University College Groningen, University of Groningen, Groningen, Netherlands

³ Centre for Theoretical Physics, The British University in Egypt, Sherouk City 11837, Cairo, Egypt

⁴Department of Physics, City College of the City University of New York, New York, NY 10031, United States

⁵Ph.D. Program in Chemistry, The Graduate Center of the City University of New York, New York, NY 10016, United States

⁶ Department of Chemistry, Yale University, New Haven, Connecticut 06520-8107, United States

⁷Department of Molecular Biophysics and Biochemistry, Yale University, New Haven, CT08620-8114

⁸ Zewail City of Science and Technology, Sheikh Zayed, District, 6th of October City, 12588 Giza, Egypt

Muhamed.amin@cfel.de

Abstract: The room temperature pump-probe X-ray free electron laser (XFEL) measurements used for serial femtosecond crystallography provide remarkable information about the structures of the catalytic (S-state) intermediates of the oxygen-evolution reaction of photosystem II. However, mixed populations of these intermediates and moderate resolution limit the interpretation of the data from current experiments. The S₃ XFEL structures show extra density near the OEC that may correspond to a water/hydroxide molecule. However, in the latest structure, this additional oxygen is 2.08 Å from the Oε2 of D1-E189, which is closer than the sum of the van der Waals radii of the two oxygens. Here, we use Boltzmann statistics and Monte Carlo sampling to provide a model for the S₂-to-S₃ state transition, allowing structural changes and the insertion of an additional water/hydroxide. Based on our model, water/hydroxide addition to the oxygen-evolving complex (OEC) is not thermodynamically favorable in the S₂ g = 2 state, but it is in the S₂ g = 4.1 redox isomer. Thus, formation of the S₃ state starts by a transition from the S₂ g = 2 to the S₂ g = 4.1 structure. Then, electrostatic interactions support protonation of D1-H190 and deprotonation of the Ca²⁺-ligated water (W3) with proton loss to the lumen. The W3 hydroxide moves toward Mn4, completing the coordination shell of Mn4 and moving with its oxidation to Mn(IV) in the S₃ state. In addition, binding additional hydroxide to Mn1 leads to a conformational change of D1-E189 in the S₂ g = 4.1 and S₃ structures. In the S₃ state in the population of protonated D1-E189 increases.

Introduction

The oxygen-evolving complex (OEC) of photosystem II (PSII) catalyzes the oxidation of water to O₂. With input of light, the OEC of PSII is sequentially oxidized. As the system is oxidized protons are lost. There are five OEC S-state intermediates along the catalytic cycle designated S₀ to S₄, with S₀ the most reduced.¹⁻⁴ The fully oxidized S₄ state catalyzes the oxidation of two waters to O₂. For understanding the reaction mechanism, it is crucial to obtain structural information about these catalytic intermediates and determine the pathway for the transitions between states.⁵⁻¹⁰

The OEC core contains a cluster of four Mn ions and a Ca²⁺ connected through bridging oxides (*i.e.*, deprotonated water molecules).¹¹ In the dark-stable S₁ state, the Mn oxidation states are (III₂, IV₂) with the subscript indicating the number of Mn ions in a given oxidation state.^{12,13} In the S₁-to-S₂ state transition, the OEC loses an electron, oxidizing an Mn(III) to Mn(IV). EPR measurements¹⁴⁻¹⁷ and theoretical models^{9,18} show two energetically accessible redox isomers of the S₂ state. When the dangler Mn4 (Figure 1) is oxidized, the Mn cluster has a total spin of S = 1/2 and produces the g = 2 multiline EPR signal (S_{2,g=2}). The second S₂ state redox isomer is formed when Mn1 (Figure 1) is oxidized and the total spin is now S = 5/2, which results in the S₂ state g = 4.1 EPR signal (S_{2,g=4.1}).^{8,9,15,17,19,20} The S₁-to-S₂ state transition is accompanied by

little or no proton loss to the lumen²¹⁻²³ and EXAFS measurements^{24,25} show no major structural rearrangements. In contrast, the S₂-to-S₃ state transition induces loss of approximately one proton/OEC and EXAFS spectra of the S₂ and S₃ states show significant structural changes.^{26,27}

Theoretical studies, recently confirmed by time-resolved XFEL structures,²⁸ show the insertion of an additional oxo/hydroxide in the S₃ state. This additional oxygen is required to complete the coordination shell of the only Mn(III) left in the S₂ state, which has only 5 ligands, facilitating its oxidation. Time-resolved photothermal beam deflection measurements suggested that this oxidation is preceded by a proton release from the OEC.^{27,29} However, it is an open question which protonatable group (amino acids/water) are releasing a proton in this transition. Although the XFEL structures are not affected by damage due to exposure to X-ray radiation, there remains disagreement about the location of this additional oxygen reported by the different XFEL studies. This results from the inhomogeneous populations of the states of the different crystals and the time point used to probe the structures.^{28,30} In addition, very high resolution is required to clearly establish the location of this oxygen near the high electron densities of the Mn ions.³¹

In the calculations reported here the position of the inserted oxygen is not fixed at the beginning of the calculation. Rather Monte Carlo sampling is used to generate a Boltzmann distribution of the possible binding sites for the oxygens of water molecules or hydroxyls, and their proton conformers in the S₂ g = 2, S₂ g = 4.1, and S₃ states and in the intermediate state where Y_Z is oxidized and its conjugate base D1-H190 is protonated (S₂-Y_Z^{*}/H190⁺).^{25,32-34} Y_Z^{*} is the electron acceptor coupled to OEC oxidation. The use of a classical, electrostatic model of the OEC enables sampling of the water/hydroxide binding sites, their protonation states and proton positions, the protonation of the amino acids and the oxidation states of the Mn centers. This method has been tested against model compounds and was used to study the proton coupled electron transfer in the Kok cycle previously.³⁵

Computational Methods

The structural model that includes amino acid residues and cofactors of PSII within a sphere with an ≈ 15 Å radius centered at the OEC cluster, two chloride ions and 85 water molecules, is optimized by QM/MM in both the g = 2 and g = 4.1 S₂ states.⁷ The geometry optimization is carried out using the ONIOM³⁶ method within the Gaussian 09³⁷ software. The amino acid residues that are included in the 15 Å sphere are: D1 (chain A): (57)-V58-V67-(68), (81)-V82-L91-(92), (107)-N108-Y112-(113), (155)-A156-I192-(193), (289)-I290-N298-(299), (323)-A324-A344/C-terminus; CP43 (chain C):(290)-W291-(292), (305)-G306-A314-(315), (334)-T335-L337-(338), (341)-M342-(343), (350)-F351-F358-(359), (398)-A399-G402-(403), (408)-G409-E413-(414); D2 (chain D):(311)-E312-L321-(322), (347)-R348-L352/C-terminus. Only backbone atoms are considered for the capped residues highlighted in parentheses. The QM region includes the Mn₄O₅Ca cluster and the amino acids ligands D1-D170, D1-E189, D1-H332, D1-E333, D1-D342, C-terminus of D1-A344, CP43-E354, D1-H337, CP43-R357, D1-D61 along with ten water molecules. The DFT/B97D³⁸⁻⁴⁰ level of theory that includes dispersion correction is used for the QM region while the AMBER^{41,42} force field is used for the MM region. The LanL2DZ^{43,44} basis set is used for calcium and manganese metal centers while 6-31G**^{45,46} is used for hydrogen, carbon, nitrogen and oxygen atoms. The capping residues, chloride ions and oxygen atoms of water molecules are frozen at the edge of the model in the MM region while all other atoms in the QM region are free to move.

Monte Carlo (MC) sampling. All water molecules except those that are ligands to Mn₄ or Ca²⁺ were removed from the QM/MM optimized structure. Then, oxygens were placed into all the cavities within 4 Å of the Mn₄O₅Ca cluster on a 1.0 Å grid using the program IPECE⁴⁷ (Figure 1A). In total, 451 oxygens were added in the cavity around the OEC. Water and hydroxide proton position conformers were generated for each oxygen atom independently (7569 hydrogen conformers were added). In addition, there is one conformer per oxygen species that represents this group moving out of the protein into solvent. Thus, each of the 451 oxygen species on the grid can be either water or hydroxide or moved to solvent in the microstates that will be subjected to MC sampling.

MCCE (Multi Conformer Continuum Electrostatics)⁴⁸ was used to generate rotamers for the side chains of the

amino acids. The electrostatic energies of the allowed conformational space are then calculated using Adaptive Poisson-Boltzmann Solver (APBS)⁴⁹ by solving the Poisson-Boltzmann equation. Based on the calculated energies, the Metropolis Monte Carlo method is used to generate the Grand Canonical Boltzmann distribution for all conformers as based on their electrostatic and van der Waals interactions at pH 7. The dielectric constant of the proteins is set to 4, and it is 80 for the solution around the sphere. The parameters for the OEC and ligands used here as reported previously in Amin et al.³

Following Grand Canonical Monte Carlo (GCMC) sampling of microstates, the structure with occupied water/hydroxyl binding sites was optimized at the DFT level using the 6-31G* basis set and the B3LYP functional. All the Mn(IV) ions were defined in the high spin state. The model included the Mn₄O₅Ca cluster and the amino acids ligands (D170, E189, H332, E333, D342, A344, CP43-E354). All amino acid residues are in the D1 protein unless otherwise noted. In addition, several other residues that interact closely with the OEC were added (D61, Y161, H190, H337, CP43-R357, G171, as well as 11 crystallographic waters including water ligands of the Mn and Ca²⁺ centers. The pK_a's of the bridging oxides were calculated in the optimized DFT model, using MCCE as described previously.^{3,18}

EXAFS simulations. EXAFS spectra of the S₃ models were computed with the FEFF program (version 6)⁵⁰ combined with the IFEFFIT code (version 1.2.12).⁵¹ We included all paths with lengths up to eight scattering legs and a Debye-Waller factor of 0.003 Å for all calculations. The energy (E) axis was converted into the photoelectron wave vector (k) space by usual transformation,

$$k = \left[\frac{2m_e}{\left(\frac{h}{2\pi}\right)^2} (E - E_0) \right]^{\frac{1}{2}},$$

where m_e is the mass of the electron and h is the Planck's constant, and $E_0 = 6540.0$ eV is the Fermi energy of Mn. A fractional cosine-square (Hanning) window with $dk = 1$ was applied to the k^3 -weighted EXAFS data. The grid of k points, which are equally spaced at 0.05 \AA^{-1} , was then used for the Fourier transformation (FT) to R space. A k range of $4.0 - 10.5 \text{ \AA}^{-1}$ was employed for the FT of the isotropic EXAFS amplitudes. In the calculation of EXAFS for different S₃ state models, we allow both the simulated intensity of the EXAFS signal and the shift in the k -space (edge shift) to relax and find the best fit using a least squares fitting procedure as done previously.¹⁰

Results and Discussions

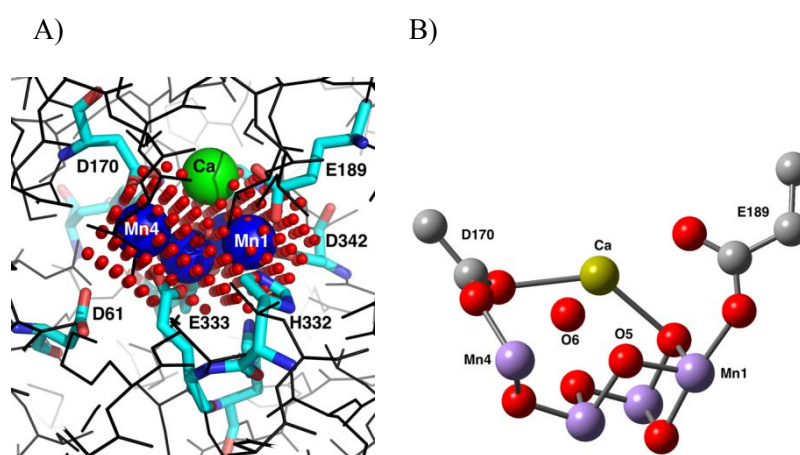


Figure 1. A) The cavity around the Mn₄O₅Ca cluster is filled with 451 oxygens that represent water molecules or hydroxyls placed on grids with 1 Å spacing. Mn are shown in blue. B) O6 is the binding site selected by MC sampling with the classical force field.

Water molecule-binding in the S_2 -to- S_3 state transition. The cavity around the Mn cluster in both the $g = 2$ and $g = 4.1$ S_2 state structures was filled with oxygen atoms of water molecules to examine the possible binding sites for an additional water/hydroxide ligand to the Mn_4O_5Ca cluster (Figure 1A). Monte Carlo sampling was used to generate a Boltzmann distribution of conformers, as defined by electrostatic and van der Waals interactions. In the S_2 $g = 2$ structure, no additional binding sites are identified nor in the S_2 $g = 2/Y_Z \cdot H190^+$ state.

However, the $Mn4-Ca^{2+}$ distance is longer by 0.27 Å in the S_2 $g = 4.1$ structure and a hydroxide (O6 Figure 1B) that bridges Mn4 and Ca^{2+} is occupied with a 25% probability, while the probability of the W3 water ligand to Ca^{2+} being present is reduced from 100% to 75%. This indicates a strong coupling so that clusters will have one or the other oxygen but never both. The transfer of W3 to the hydroxide, O6 position, is coupled to the loss of a proton. The O6 oxygen is located 2.06 Å from Mn4, 2.22 Å from Ca^{2+} and 1.78 Å from O5. In the S_2 $g = 4.1/Y_Z \cdot H190^+$ state, now O6 is always present and W3 is never found in accepted microstates, which suggests a proton loss upon the formation of $Y_Z \cdot H190^+$, before oxidation of the Mn cluster. This sequence of events has been observed by time-resolved photothermal beam deflection measurements.²⁷ The total charge of the protein upon the formation of $Y_Z \cdot H190^+$ is reduced by one unit, which suggests that a proton is released to the lumen.

Cluster based DFT calculations⁵⁴ also suggested that the binding of an additional water molecule takes place at Mn1 in the $g = 2$ form of the S_2 state, a transition that is at high energy here. A similar mechanism in which W3 deprotonates and translates to complete the coordination shell of Mn4 has been proposed by Ugur et al.⁵² However, they also proposed that W3 may translate toward Mn1 in the S_2 $g = 2$ structure to complete its coordination shell. This is included as a possible transition but is found to be energetically unfavorable in our simulations. Earlier computational studies generally agree that the water/hydroxide is inserted into the OEC cluster from the closed, S_2 state $g = 4.1$ structure.^{8,19,32,53} The S_2 state $g = 4.1$ form is less rigid, with higher fluctuations that allow the rearrangement needed for binding an additional water molecule.⁸

The two S_2 structures were then advanced to the S_3 state to oxidize the Mn centers by changing the redox potential (E_h), at physiological pH where:

$$\Delta G^{Mn(III-IV)} = [F(E_h - E_{m,sol})] + \Delta \Delta G_{solvation} + \Delta \Delta G_{pairwise}$$

where $\Delta G^{Mn(III-IV)}$ is the energy required to oxidize an isolated Mn center from Mn(III) to Mn(IV), F is the Faraday constant, $E_{m,sol}$ is the mid-point reduction potential of Mn(IV) in solution as obtained in Amin et al.,³⁵ $\Delta \Delta G_{solvation}$ is the desolvation penalty of Mn4 and $\Delta \Delta G_{pairwise}$ is the pairwise electrostatic interaction between Mn and the surrounding residues, waters, Ca^{2+} and bridging oxygen atoms.

In the S_2 $g = 4.1$ structure, Mn4 is oxidized at 0.6 V and the oxidation is coupled to binding O6, while in the S_2 $g = 2$ structure Mn1 has a potential for oxidation of 1.4 V, which is higher than the potential for oxidation of P680. This suggests the advancement of the OEC to the S_3 state through the S_2 $g = 2$ state is energetically unfavorable, which agrees with earlier studies.^{8,19,32,53,55-57} Thus, for the OEC to advance from the S_2 $g = 2$ state to the S_3 state, it has to transit through the S_2 $g = 4.1$ state.⁵⁸⁻⁶⁰ Experimental studies using EPR spectroscopy^{58,59} also indicates the formation of the S_3 state from the S_2 state $g = 4.1$ isomer at lower temperatures in both Ca-PSII and Sr-PSII. Combined multiscale *ab initio* DFT+U simulations¹⁹ suggested that the oxidation of Y_Z stabilizes the conversion of the open form ($g = 2$) to closed ($g = 4.1$) S_2 state isomer prior to formation of the S_3 state.

The analysis thus far has used a classical force field to extensively sample many oxygen and proton positions of water molecules. The S_3 structure with the additional hydroxide in the O6 position, obtained by MC sampling with only electrostatic and van der Waals interactions, was optimized by using DFT. The optimization adjusted the position of O6 to complete the octahedral coordination shell of Mn4 (Figure 1B), reducing the Mn4-O6 bond to 1.91 Å, while the Ca^{2+} -O6 and O6-O5 distances increased to 2.46 Å and 2.74 Å, respectively. Upon optimization, an additional hydrogen bond was formed between the hydroxide O6 and μ -oxo O5 with a distance of 2.30 Å.

There are two structural models of the S_3 state proposed in the literature, with “open” or “closed” structures of the Mn_4O_5Ca cubane that may be relevant for the catalytic reaction.^{10,61–64} In the closed cubane structure, O6-H is placed 3.57 Å away from Ca^{2+} and does not form a hydrogen bond with O5. In the open structure, O6 is located at 2.97 Å from Ca^{2+} forming a strong hydrogen bond with O5. The model proposed in this paper is an intermediate between the closed and open models of the S_3 state, with O6 forming a hydrogen bond with O5 but not as strongly as in the earlier open structure model. In addition, the O6- Ca^{2+} distance is shorter in our model than the other two forms (Figure S1).

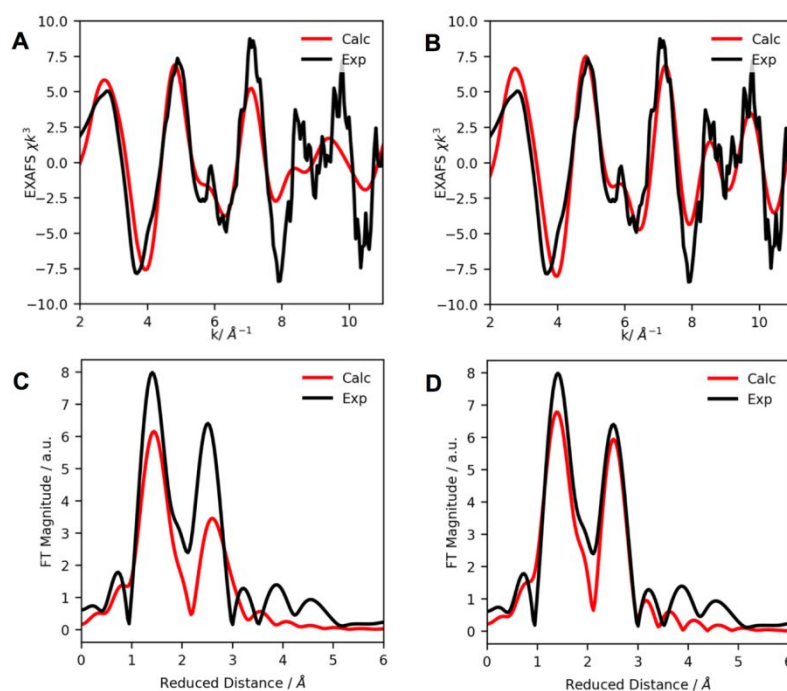


Figure 2. Comparison of calculated (red) and experimental (black) Mn EXAFS spectra of different S_3 state models in k -space (A and B) and reduced distance space (C and D) for the new model obtained in this study (A and C) and the previous QM/MM-optimized open form of the S_3 state (B and D).¹⁰

Figure 2 compares the EXAFS spectrum of the S_3 state model obtained in the current study (panels A and C) with the corresponding spectrum of the previously reported QM/MM S_3 model (panels B and D) and the experimental EXAFS data.⁶⁵ The comparison suggests that the S_3 state model obtained in the current study does not match the experimental EXAFS data as well as the QM/MM-optimized open-form of the S_3 state, suggesting that the structure we obtained in this study may be an intermediate structure during the S_2 -to- S_3 state transition, with the final metastable S_3 state best described as the open form of the S_3 state. The largest difference in the Fourier Transformed spectrum is observed for the second peak (Figure 2 C, D), i.e. the Mn-Mn/Mn- Ca^{2+} distances, which are sensitive to the different positions of the additional ligand O6 (Figure S1).

Role of D1-E189. While D1-E189 appears to be a ligand of Mn1 in the S_1 dark-adapted state, FTIR difference spectroscopy suggested that it is not a ligand of a Mn that undergoes oxidation between the S_0 and S_3 state transitions.⁶⁶ In addition, the recently published 2.07 Å resolution S_3 state structure by Kern et al.²⁸ showed a translation of E189 away from Mn1 upon the insertion of a water molecule that is only 2.09 Å away from O5 and 1.78 Å from Mn1. Thus, to examine the role of E189, we have generated more than 50 conformers of its sidechains and sampled them along with 451 water molecule-binding sites in the S_2 $g = 2$, S_2 $g = 4.1$ and S_3 states.

The MC sampling confirms a conformational change for E189 moving away from Mn1 that is coupled to binding another OH^- (O7) i.e., O7 replacing the anionic E189 as a ligand for Mn1. These conformational changes are coupled to the oxidation of Mn1 in both the S_2 state $g = 4.1$ and the S_3 state structures while no conformational changes were observed for the S_2 state $g = 2$ structure. Although the XFEL structures show different conformations of E189, the conformational

changes observed in our simulations are larger than the reported in the XFEL structures and suggest a complete loss of coordination of E189 from Mn1, which is replaced by a hydroxyl.

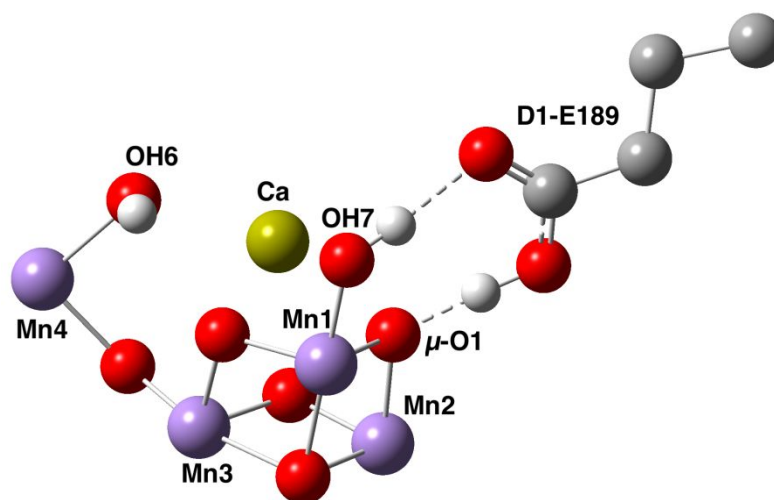


Figure 3. The ligand environment of Mn1 with O7 (hydroxyl anion) and protonated D1-E189. Strong hydrogen bonds (shown in dashed lines) are formed between D1-E189, OH7 and μ -O1.

The OH7 (i.e., the hydroxyl anion form of O7) has a stronger dipole moment than the carboxylate group of the amino acid and replaces the E189 ligand in the S_2 $g = 4.1$ and in the S_3 state due to the electrostatic attraction with Mn1. However, in the S_2 $g = 2$ state, Mn1 is in the Mn(III) state and the repulsion with the nearby oxo bridges and negatively charged ligands is stronger than the attraction to Mn1. Thus, in the S_1 and S_2 $g = 2$ states E189 is a Mn1 ligand and no OH⁻ binds to Mn1. O7 binding is independent from the addition of O6, i.e. both hydroxides may bind the OEC simultaneously. However, when O7 has replaced E189 as the Mn1 ligand, the protonation state of E189 is dependent on the state of O6. Thus, E189 is ionized in the S_2 $g = 4.1$ state because O6 is not bound yet to the cluster; instead, the Ca²⁺ ligand W3 is mostly occupied. In the S_3 state, O6 binds to the cluster and causes an approximately 50:50 mixture of protonated and deprotonated E189 due to the electrostatic repulsions.

To further assess the energetics of O7 binding, we compared the optimized DFT energies of the S_3 state having E189 ionized and bound to Mn1 (Mn1-E189) with the S_3 state having OH7 bound to Mn1 and protonated E189 (Mn1-OH7). The X, Y, Z coordinates of the two optimized structures, the DFT energies (in Hartree) and the Mn spin densities are reported in the SI (Table S1). The Mn1-OH7 structure energy is 2.4 kcal/mol lower than the Mn1-E189 structure, which indicates that the two states are close in energy, in agreement with the MC sampling calculations. The mutations of E189 (E189K, R and Q) have shown no effect on electron transfer at the donor side of photosystem II,⁶⁷ which may be explained by the existence of an isoenergetic structure (Mn1-OH7) that facilitates the oxidation of Mn1 through the Kok cycle.

XFEL structures of the S_3 state.

The optimized Mn1-OH7 structure shows strong hydrogen bonds formed between O7, the carboxylate group of E189 (2.83 Å O-O distance) and the μ -oxo that bridges Mn1 and Mn2 (Figure 3). The position of O7 is very similar to the additional oxygen resolved in the latest S_3 structure Kern et al.²⁸ (Table 1). However, the Kern et al. structure **also** has an unusually short inter-atomic distance of 2.08 Å between the newly inserted oxygen and Oe2 of E189, which is much shorter than the sum of their van der Waals radii, and is considered to be physically impossible. Such a short distance cannot be rationalized with any known repulsive force field parameters in molecular dynamic simulation. If O7 is coordinated as a ligand of Mn1, E189 must move away from O7 through repulsive interactions with E189. It is interesting that E189 always has multiple conformations in both the Suga et al. and Kern et al. S_3 structures. Furthermore, Kern et al. have built two conformations for E189, and in the second of these the O7- Oe2 E189 distance is 1.60 Å. This suggests that O7 and E189 are mutually exclusive in space in this conformation. It is relatively straightforward to detect the binding of a water molecule

in a location where nothing is there using F_o-F_o isomorphous difference Fourier maps regardless of its low population. However, it is much more challenging to establish a displacement of side chains such as E189 using the same method, which may become undetectable when the population is low. This may explain the uncertainties in the sidechain positions of E189.

The S_3 XFEL structure by Suga et al. at 2.25 Å resolution suggested the insertion of an additional oxygen (or water substrate) that is only 1.46 Å away from O5 similar to the S_3 open structure.⁶⁸ However, this short distance between the two oxygens is possible only when there is H atom trapped between them and may have resulted from superposition of states with lower oxidation levels.⁶⁹ The O6 position observed in the Suga et al. S_3 structure is far from E189. Even so, possible multiple conformations of E189 in the S_3 state have been detected (for example, Figure S5 of Wang⁷⁰ et al., 2017). Therefore, the possibility of a third E189 conformation as proposed by this study does not contradict the evidence of the structure given the current uncertainty.

Table 1 shows the comparison of the $Mn_i, Ca^{2+}-O_j$ ($i = 1,4$ and $j = 5,6,7$) distances in the different structures. It is clear that the position of O6 is similar to the oxygen position observed in the XFEL structure by Suga et al.,³⁰ while the position of O7 is closer to the oxygen identified in the S_3 structure by Kern et al.²⁸ The mismatch between the XFEL measurements may have resulted from the uncertainties in the oxygen positions, due to the difficulties of accurately resolving their electron density near the heavy Mn ions, the fact that misses in a multi-flash experiment will produce a mixture of S states, the different time points used to probe the structures, and the changes induced by radiation.^{71,72}

Table 1. The distances in the optimized $S_{2g=2}$, $S_{2g=4.1}$ and S_3 structures.

	$S_{2g=2}$	$S_{2g=4.1}$	S_{3Suga}	S_{3Kern}	S_{3-DFT}
Mn1-Ca ²⁺	3.30	2.87	3.26	3.33	2.92
Mn4-Ca ²⁺	3.93	4.20	4.07	3.90	3.93
Mn1-O5	2.96	1.83	2.80	2.90	1.84
Mn4-O5	1.82	2.99	3.51	2.26	3.35
Mn1-O6	-	-	2.27	-	4.26
Mn4-O6	-	-	2.30	-	1.97
Mn1-O7	-	-	-	1.78	1.79
Mn4-O7	-	-	-	4.18	5.74
O5-O6	-	-	1.46	2.09	2.65
O5-O7	-	-	-	2.10	2.75
O6-O7	-	-	-	-	4.29

All distances are in Å. No binding sites identified for O6 or O7 in the $S_{2g=2}$ structure. The S_{3Suga} ⁶⁸ structure is resolved at 2.5 Å (PDB ID:5GTI), while the S_{3Kern} ²⁸ is resolved at 2.07 Å (PDB ID:6DHO).

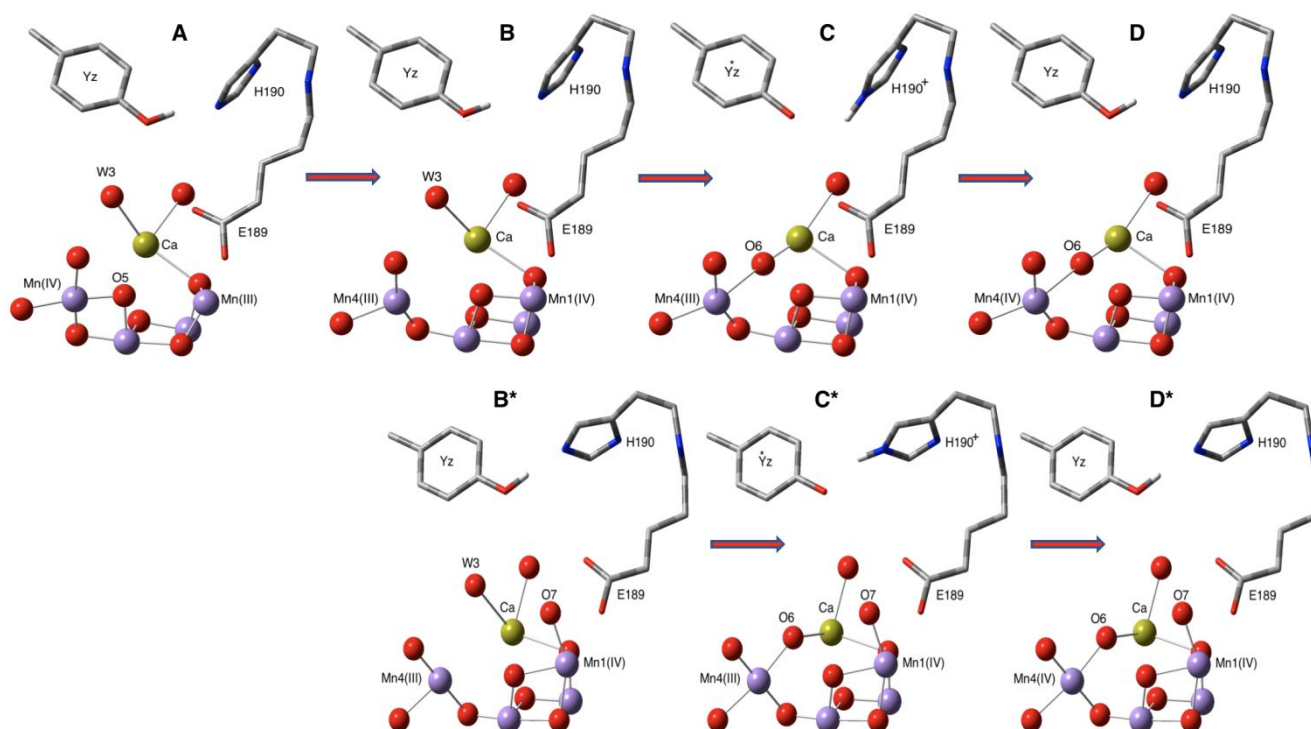


Figure 4. The proposed mechanism for the S_2 -to- S_3 state transition. A, B, C and D are the S_2 $g = 2$, S_2 $g = 4.1$, S_2 $g = 4.1/Y_Z \cdot H190^+$ and S_3 states, respectively. The reaction starts at A (S_2 $g = 2$) and ends at D (S_3). The B^* , C^* and D^* are possible isomers of the B, C and D states, where O7 replaces D1-E189 as a ligand for Mn1.

Conclusions

Simulations based on classical Monte Carlo sampling of many possible oxygen positions to generate the Boltzmann distribution suggest the transition from the S_2 to the S_3 state starts by a transition from the S_2 $g = 2$ state to the S_2 $g = 4.1$ state. Then, W3 on calcium deprotonates upon the formation of the $Y_Z \cdot H190^+$ intermediate prior to the oxidation of the Mn cluster. The deprotonation of W3 is coupled to a translation of the oxygen toward Mn4, which completes its coordination shell and facilitates the oxidation of the cluster to the S_3 state (Figure 4). The EXAFS spectrum of the resulting S_3 state structure suggests it is more consistent with an intermediate generated during the S_2 -to- S_3 state transition prior to formation of the S_3 state in its open form.¹⁰ In addition, the sampling of several conformers of the D1-E189 sidechain suggest that it undergoes a conformational change that is coupled to the oxidation of Mn1 and the binding another OH^- (O7) as suggested by the latest XFEL S_3 state structure (Figure 4, B^* , C^* , D^*).

Supporting Information

The Supporting Information includes Mn spin densities and the optimized atomic coordinates of the proposed models of the S_3 state.

Acknowledgements

The authors acknowledge computational resources from NERSC (V.S.B.) and support by the U.S. Department of Energy, Office of Science, Office of Basic Energy Sciences, Division of Chemical Sciences, Geosciences, and Biosciences via Grants DESC0001423 (M.R.G. and V.S.B.), DE-FG02-05ER15646 (G.W.B.) and from European Research Council through the Consolidator Grant COMOTION (ERC-Küpper-614507).

References:

- (1) Kok, B.; Forbush, B.; McGloin, M. Cooperation of Charges in Photosynthetic O₂ Evolution-I. A Linear Four Step Mechanism. *Photochem. Photobiol.* **1970**, *11* (6), 457–475.
- (2) Brudvig, G. W. Water Oxidation Chemistry of Photosystem II. *Philos Trans R Soc Lond B Biol Sci* **2008**, *363* (1494), 1211–1219. <https://doi.org/10.1098/rstb.2007.2217>.
- (3) Amin, M.; Vogt, L.; Szejgis, W.; Vassiliev, S.; Brudvig, G. W.; Bruce, D.; Gunner, M. R. Proton-Coupled Electron Transfer during the S-State Transitions of the Oxygen-Evolving Complex of Photosystem II. *J. Phys. Chem. B* **2015**, *119* (24), 7366–7377. <https://doi.org/10.1021/jp510948e>.
- (4) Dau, H.; Haumann, M. The Manganese Complex of Photosystem II in Its Reaction Cycle—Basic Framework and Possible Realization at the Atomic Level. *Coord. Chem. Rev.* **2008**, *252* (3–4), 273–295. <https://doi.org/10.1016/j.ccr.2007.09.001>.
- (5) Pal, R.; Negre, C. F.; Vogt, L.; Pokhrel, R.; Ertem, M. Z.; Brudvig, G. W.; Batista, V. S. S₀-State Model of the Oxygen-Evolving Complex of Photosystem II. *Biochemistry* **2013**, *52* (44), 7703–7706. <https://doi.org/10.1021/bi401214v>.
- (6) Luber, S.; Rivalta, I.; Umena, Y.; Kawakami, K.; Shen, J.-R.; Kamiya, N.; Brudvig, G. W.; Batista, V. S. S₁-State Model of the O₂-Evolving Complex of Photosystem II. *Biochemistry* **2011**, *50* (29), 6308–6311. <https://doi.org/10.1021/bi200681q>.
- (7) Askerka, M.; Wang, J.; Brudvig, G. W.; Batista, V. S. Structural Changes in the Oxygen-Evolving Complex of Photosystem II Induced by the S₁ to S₂ Transition: A Combined XRD and QM/MM Study. *Biochemistry* **2014**, *53* (44), 6860–6862. <https://doi.org/10.1021/bi5011915>.
- (8) Bovi, D.; Narzi, D.; Guidoni, L. The S₂ State of the Oxygen-Evolving Complex of Photosystem II Explored by QM/MM Dynamics: Spin Surfaces and Metastable States Suggest a Reaction Path towards the S₃ State. *Angew. Chem.* **2013**, *52* (45), 11744–11749. <https://doi.org/10.1002/anie.201306667>.
- (9) Pantazis, D. A.; Ames, W.; Cox, N.; Lubitz, W.; Neese, F. Two Interconvertible Structures That Explain the Spectroscopic Properties of the Oxygen-evolving Complex of Photosystem II in the S₂ State. *Angew. Chem.* **2012**, *51* (39), 9935–9940. <https://doi.org/10.1002/anie.201204705>.
- (10) Askerka, M.; Wang, J.; Vinyard, D. J.; Brudvig, G. W.; Batista, V. S. S₃ State of the O₂-Evolving Complex of Photosystem II: Insights from QM/MM, EXAFS, and Femtosecond X-Ray Diffraction. *Biochemistry* **2016**, *55* (7), 981–984. <https://doi.org/10.1021/acs.biochem.6b00041>.
- (11) Umena, Y.; Kawakami, K.; Shen, J.-R.; Kamiya, N. Crystal Structure of Oxygen-Evolving Photosystem II at a Resolution of 1.9 Å. *Nature* **2011**, *473* (7345), 55–60. <https://doi.org/10.1038/nature09913>.
- (12) Lohmiller, T.; Ames, W.; Lubitz, W.; Cox, N.; Misra, S. K. EPR Spectroscopy and the Electronic Structure of the Oxygen-Evolving Complex of Photosystem II. *Appl Magn Reson* **2013**, *44* (6), 691–720. <https://doi.org/10.1007/s00723-012-0437-3>.
- (13) Britt, R. D.; Campbell, K. A.; Peloquin, J. M.; Gilchrist, M. L.; Aznar, C. P.; Dicus, M. M.; Robblee, J.; Messinger, J. Recent Pulsed EPR Studies of the Photosystem II Oxygen-Evolving Complex: Implications as to Water Oxidation Mechanisms. *Biochim Biophys Acta Bioenerg* **2004**, *1655*, 158–171. <https://doi.org/10.1016/j.bbabi.2003.11.009>.
- (14) Dismukes, G. C.; Siderer, Y. Intermediates of a Polynuclear Manganese Center Involved in Photosynthetic Oxidation of Water. *Proc. Natl. Acad. Sci. U.S.A.* **1981**, *78* (1), 274–278. <https://doi.org/10.1073/pnas.78.1.274>.
- (15) Zimmermann, J. L.; Rutherford, A. W. EPR Studies of the Oxygen-Evolving Enzyme of Photosystem II. *Biochim Biophys Acta Bioenerg* **1984**, *767* (1), 160–167. [https://doi.org/10.1016/0005-2728\(84\)90091-4](https://doi.org/10.1016/0005-2728(84)90091-4).
- (16) de Paula, J. C.; Brudvig, G. W. Magnetic Properties of Manganese in the Photosynthetic Oxygen-Evolving Complex. *J. Am. Chem. Soc.* **1985**, *107* (9), 2643–2648. <https://doi.org/10.1021/ja00295a016>.
- (17) Casey, J. L.; Sauer, K. EPR Detection of a Cryogenically Photogenerated Intermediate in Photosynthetic Oxygen Evolution. *Biochim. Biophys. Acta* **1984**, *767* (1), 21–28. [https://doi.org/10.1016/0005-2728\(84\)90075-6](https://doi.org/10.1016/0005-2728(84)90075-6).

- (18) Amin, M.; Pokhrel, R.; Brudvig, G. W.; Badawi, A.; Obayya, S. S. A. Effect of Chloride Depletion on the Magnetic Properties and the Redox Leveling of the Oxygen-Evolving Complex in Photosystem II. *J. Phys. Chem. B* **2016**, *120* (18), 4243–4248. <https://doi.org/10.1021/acs.jpcc.6b03545>.
- (19) Narzi, D.; Bovi, D.; Guidoni, L. Pathway for Mn-Cluster Oxidation by Tyrosine-Z in the S₂ State of Photosystem II. *Proc. Natl. Acad. Sci. U.S.A.* **2014**, *111* (24), 8723–8728. <https://doi.org/10.1073/pnas.1401719111>.
- (20) Ono, T.; Zimmermann, J. L.; Inoue, Y.; Rutherford, A. W. EPR Evidence for a Modified S-State Transition in Chloride-Depleted Photosystem II. *Biochim Biophys Acta Bioenerg* **1986**, *851* (2), 193–201. [https://doi.org/10.1016/0005-2728\(86\)90125-8](https://doi.org/10.1016/0005-2728(86)90125-8).
- (21) Rappaport, F.; Lavergne, J. Proton Release during Successive Oxidation Steps of the Photosynthetic Water Oxidation Process: Stoichiometries and PH Dependence. *Biochemistry* **1991**, *30* (41), 10004–10012. <https://doi.org/10.1021/bi00105a027>.
- (22) Lavergne, J.; Junge, W. Proton Release during the Redox Cycle of the Water Oxidase. *Photosynth Res* **1993**, *38* (3), 279–296. <https://doi.org/10.1007/BF00046752>.
- (23) Suzuki, H.; Sugiura, M.; Noguchi, T. Monitoring Proton Release during Photosynthetic Water Oxidation in Photosystem II by Means of Isotope-Edited Infrared Spectroscopy. *J. Am. Chem. Soc.* **2009**, *131* (22), 7849–7857. <https://doi.org/10.1021/ja901696m>.
- (24) Yano, J.; Pushkar, Y.; Glatzel, P.; Lewis, A.; Sauer, K.; Messinger, J.; Bergmann, U.; Yachandra, V. High-Resolution Mn EXAFS of the Oxygen-Evolving Complex in Photosystem II: Structural Implications for the Mn₄Ca Cluster. *J. Am. Chem. Soc.* **2005**, *127* (43), 14974–14975. <https://doi.org/10.1021/ja054873a>.
- (25) Askerka, M.; Brudvig, G. W.; Batista, V. S. The O₂-Evolving Complex of Photosystem II: Recent Insights from Quantum Mechanics/Molecular Mechanics (QM/MM), Extended X-Ray Absorption Fine Structure (EXAFS), and Femtosecond X-Ray Crystallography Data. *Acc. Chem. Res.* **2017**, *50* (1), 41–48. <https://doi.org/10.1021/acs.accounts.6b00405>.
- (26) Dau, H.; Grundmeier, A.; Loja, P.; Haumann, M. On the Structure of the Manganese Complex of Photosystem II: Extended-Range EXAFS Data and Specific Atomic-Resolution Models for Four S-States. *Philos Trans R Soc Lond B Biol Sci* **2008**, *363* (1494), 1237–1244. <https://doi.org/10.1098/rstb.2007.2220>.
- (27) Zaharieva, I.; Dau, H.; Haumann, M. Sequential and Coupled Proton and Electron Transfer Events in the S₂ → S₃ Transition of Photosynthetic Water Oxidation Revealed by Time-Resolved X-Ray Absorption Spectroscopy. *Biochemistry* **2016**, *55* (50), 6996–7004. <https://doi.org/10.1021/acs.biochem.6b01078>.
- (28) Kern, J.; Chatterjee, R.; Young, I. D.; Fuller, F. D.; Lassalle, L.; Ibrahim, M.; Gul, S.; Fransson, T.; Brewster, A. S.; Alonso-Mori, R.; et al. Structures of the Intermediates of Kok's Photosynthetic Water Oxidation Clock. *Nature* **2018**, *563* (7731), 421–425. <https://doi.org/10.1038/s41586-018-0681-2>.
- (29) Dau, H.; Zaharieva, I.; Haumann, M. Recent Developments in Research on Water Oxidation by Photosystem II. *Curr Opin Chem Biol* **2012**, *16* (1–2), 3–10. <https://doi.org/10.1016/j.cbpa.2012.02.011>.
- (30) Suga, M.; Akita, F.; Hirata, K.; Ueno, G.; Murakami, H.; Nakajima, Y.; Shimizu, T.; Yamashita, K.; Yamamoto, M.; Ago, H.; et al. Native Structure of Photosystem II at 1.95 Å Resolution Viewed by Femtosecond X-Ray Pulses. *Nature* **2015**, *517* (7532), 99–103. <https://doi.org/10.1038/nature13991>.
- (31) Askerka, M.; Vinyard, D. J.; Wang, J.; Brudvig, G. W.; Batista, V. S. Analysis of the Radiation-Damage-Free X-Ray Structure of Photosystem II in Light of EXAFS and QM/MM Data. *Biochemistry* **2015**, *54* (9), 1713–1716. <https://doi.org/10.1021/acs.biochem.5b00089>.
- (32) Retegan, M.; Krewald, V.; Mamedov, F.; Neese, F.; Lubitz, W.; Cox, N.; Pantazis, D. A. A Five-Coordinate Mn(IV) Intermediate in Biological Water Oxidation: Spectroscopic Signature and a Pivot Mechanism for Water Binding. *Chem. Sci.* **2015**, *7* (1), 72–84. <https://doi.org/10.1039/C5SC03124A>.
- (33) Cox, N.; Messinger, J. Reflections on Substrate Water and Dioxygen Formation. *Biochim. Biophys. Acta* **2013**, *1827* (8), 1020–1030. <https://doi.org/10.1016/j.bbabi.2013.01.013>.
- (34) Siegbahn, P. E. M. Substrate Water Exchange for the Oxygen Evolving Complex in PSII in the S₁, S₂, and S₃ States. *J. Am. Chem. Soc.* **2013**, *135* (25), 9442–9449. <https://doi.org/10.1021/ja401517e>.

- (35) Amin, M.; Vogt, L.; Vassiliev, S.; Rivalta, I.; Sultan, M. M.; Bruce, D.; Brudvig, G. W.; Batista, V. S.; Gunner, M. R. Electrostatic Effects on Proton Coupled Electron Transfer in Oxomanganese Complexes Inspired by the Oxygen-Evolving Complex of Photosystem II. *J Phys Chem B* **2013**, *117* (20), 6217–6226. <https://doi.org/10.1021/jp403321b>.
- (36) Vreven, T.; Morokuma, K. The ONIOM (Our Own N-Layered Integrated Molecular Orbital + Molecular Mechanics) Method for the First Singlet Excited (S_1) State Photoisomerization Path of a Retinal Protonated Schiff Base. *J. Chem. Phys.* **2000**, *113* (8), 2969–2975. <https://doi.org/10.1063/1.1287059>.
- (37) Frisch, M. J.; Trucks, G. W.; Schlegel, H. B.; Scuseria, G. E.; Robb, M. A.; Cheeseman, J. R.; Scalmani, G.; Barone, V.; Petersson, G. A.; Nakatsuji, H.; et al. G09 | Gaussian.Com. **2016**.
- (38) Becke, A. D. Density-Functional Exchange-Energy Approximation with Correct Asymptotic Behavior. *Phys. Rev. A* **1988**, *38* (6), 3098–3100. <https://doi.org/10.1103/PhysRevA.38.3098>.
- (39) Becke, A. D. Density-functional Thermochemistry. III. The Role of Exact Exchange. *J. Chem. Phys.* **1993**, *98* (7), 5648–5652. <https://doi.org/10.1063/1.464913>.
- (40) Grimme, S. Semiempirical GGA-Type Density Functional Constructed with a Long-Range Dispersion Correction. *J. Comput. Chem.* **2006**, *27* (15), 1787–1799. <https://doi.org/10.1002/jcc.20495>.
- (41) Case, D. A.; Darden, T. A.; Cheatham, T. E.; Simmerling, C. L.; Wang, J.; Duke, R. E.; Luo, R.; Walker, R. C.; Zhang, W.; Merz, K. M.; et al. AMBER 12, University of California, San Francisco.
- (42) Cornell, W. D.; Cieplak, P.; Bayly, C. I.; Gould, I. R.; Merz, K. M.; Ferguson, D. M.; Spellmeyer, D. C.; Fox, T.; Caldwell, J. W.; Kollman, P. A. A Second Generation Force Field for the Simulation of Proteins, Nucleic Acids, and Organic Molecules. *J. Am. Chem. Soc.* **1995**, *117* (19), 5179–5197. <https://doi.org/10.1021/ja00124a002>.
- (43) Hay, P. J.; Wadt, W. R. Ab Initio Effective Core Potentials for Molecular Calculations. Potentials for K to Au Including the Outermost Core Orbitals. *J. Chem. Phys.* **1985**, *82* (1), 299–310. <https://doi.org/10.1063/1.448975>.
- (44) Wadt, W. R.; Hay, P. J. Ab Initio Effective Core Potentials for Molecular Calculations. Potentials for Main Group Elements Na to Bi. *J. Chem. Phys.* **1985**, *82* (1), 284–298. <https://doi.org/10.1063/1.448800>.
- (45) Ditchfield, R.; Hehre, W. J.; Pople, J. A. Self-consistent Molecular-orbital Methods. IX. An Extended Gaussian-type Basis for Molecular-orbital Studies of Organic Molecules. *J. Chem. Phys.* **1971**, *54* (2), 724–728. <https://doi.org/10.1063/1.1674902>.
- (46) Hariharan, P. C.; Pople, J. A. The Influence of Polarization Functions on Molecular Orbital Hydrogenation Energies. *Theoret. Chim. Acta* **1973**, *28* (3), 213–222. <https://doi.org/10.1007/BF00533485>.
- (47) Song, Y.; Gunner, M. R. Using Multiconformation Continuum Electrostatics to Compare Chloride Binding Motifs in α -Amylase, Human Serum Albumin, and Omp32. *J. Mol. Biol.* **2009**, *387* (4), 840–856. <https://doi.org/10.1016/j.jmb.2009.01.038>.
- (48) Song, Y.; Mao, J.; Gunner, M. R. MCCE2: Improving Protein PK_a Calculations with Extensive Side Chain Rotamer Sampling. *J. Comput. Chem.* **2009**, *30* (14), 2231–2247. <https://doi.org/10.1002/jcc.21222>.
- (49) Baker, N. A.; Sept, D.; Joseph, S.; Holst, M. J.; McCammon, J. A. Electrostatics of Nanosystems: Application to Microtubules and the Ribosome. *Proc. Natl. Acad. Sci. U.S.A.* **2001**, *98* (18), 10037–10041. <https://doi.org/10.1073/pnas.181342398>.
- (50) Rehr, J. J.; Albers, R. C. Theoretical Approaches to X-Ray Absorption Fine Structure. *Rev. Mod. Phys.* **2000**, *72* (3), 621–654. <https://doi.org/10.1103/RevModPhys.72.621>.
- (51) Newville, M. EXAFS Analysis Using FEFF and FEFFIT. *J Synchrotron Rad* **2001**, *8* (2), 96–100. <https://doi.org/10.1107/S0909049500016290>.
- (52) Ugur, I.; Rutherford, A. W.; Kaila, V. R. I. Redox-Coupled Substrate Water Reorganization in the Active Site of Photosystem II—The Role of Calcium in Substrate Water Delivery. *Biochim Biophys Acta Bioenerg* **2016**, *1857* (6), 740–748. <https://doi.org/10.1016/j.bbabi.2016.01.015>.
- (53) Capone, M.; Narzi, D.; Bovi, D.; Guidoni, L. Mechanism of Water Delivery to the Active Site of Photosystem II along the S_2 to S_3 Transition. *J. Phys. Chem. Lett.* **2016**, *7* (3), 592–596. <https://doi.org/10.1021/acs.jpcclett.5b02851>.

- (54) Siegbahn, P. E. M. Mechanisms for Proton Release during Water Oxidation in the S_2 to S_3 and S_3 to S_4 Transitions in Photosystem II. *Phys. Chem. Chem. Phys.* **2012**, *14* (14), 4849–4856. <https://doi.org/10.1039/C2CP00034B>.
- (55) Guo, Y.; Li, H.; He, L.-L.; Zhao, D.-X.; Gong, L.-D.; Yang, Z.-Z. Theoretical Reflections on the Structural Polymorphism of the Oxygen-Evolving Complex in the S_2 State and the Correlations to Substrate Water Exchange and Water Oxidation Mechanism in Photosynthesis. *Biochim Biophys Acta Bioenerg* **2017**, *1858* (10), 833–846. <https://doi.org/10.1016/j.bbabi.2017.08.001>.
- (56) Shoji, M.; Isobe, H.; Yamaguchi, K. QM/MM Study of the S_2 to S_3 Transition Reaction in the Oxygen-Evolving Complex of Photosystem II. *Chem. Phys. Lett.* **2015**, *636*, 172–179. <https://doi.org/10.1016/j.cplett.2015.07.039>.
- (57) Beal, N. J.; Corry, T. A.; O'Malley, P. J. A Comparison of Experimental and Broken Symmetry Density Functional Theory (BS-DFT) Calculated Electron Paramagnetic Resonance (EPR) Parameters for Intermediates Involved in the S_2 to S_3 State Transition of Nature's Oxygen Evolving Complex. *J. Phys. Chem. B* **2018**, *122* (4), 1394–1407. <https://doi.org/10.1021/acs.jpcc.7b10843>.
- (58) Boussac, A.; Rutherford, A. W.; Sugiura, M. Electron Transfer Pathways from the S_2 -States to the S_3 -States Either after a Ca^{2+}/Sr^{2+} or a Cl^-/I^- Exchange in Photosystem II from *Thermosynechococcus Elongatus*. *Biochim. Biophys. Acta* **2015**, *1847* (6), 576–586. <https://doi.org/10.1016/j.bbabi.2015.03.006>.
- (59) Boussac, A.; Ugur, I.; Marion, A.; Sugiura, M.; Kaila, V. R. I.; Rutherford, A. W. The Low Spin - High Spin Equilibrium in the S_2 -State of the Water Oxidizing Enzyme. *Biochim Biophys Acta Bioenerg* **2018**, *1859* (5), 342–356. <https://doi.org/10.1016/j.bbabi.2018.02.010>.
- (60) Kaur, D.; Szejgis, W.; Mao, J.; Amin, M.; Reiss, K. M.; Askerka, M.; Cai, X.; Khaniya, U.; Zhang, Y.; Brudvig, G. W.; et al. Relative Stability of the S_2 Isomers of the Oxygen Evolving Complex of Photosystem II. *Photosyn. Res.* **2019**. <https://doi.org/10.1007/s11120-019-00637-6>.
- (61) Blomberg, M. R. A.; Siegbahn, P. E. M. A Quantum Chemical Study of Tyrosyl Reduction and O—O Bond Formation in Photosystem II. *Mol. Phys.* **2003**, *101* (1–2), 323–333. <https://doi.org/10.1080/00268970210162781>.
- (62) Limburg, J.; Vrettos, J. S.; Liable-Sands, L. M.; Rheingold, A. L.; Crabtree, R. H.; Brudvig, G. W. A Functional Model for O-O Bond Formation by the O_2 -Evolving Complex in Photosystem II. *Science* **1999**, *283* (5407), 1524–1527. <https://doi.org/10.1126/science.283.5407.1524>.
- (63) Siegbahn, P. E. M. O-O Bond Formation in the S_4 State of the Oxygen-Evolving Complex in Photosystem II. *Chem. Eur. J.* **2006**, *12* (36), 9217–9227. <https://doi.org/10.1002/chem.200600774>.
- (64) Cox, N.; Retegan, M.; Neese, F.; Pantazis, D. A.; Boussac, A.; Lubitz, W. Electronic Structure of the Oxygen-Evolving Complex in Photosystem II Prior to O-O Bond Formation. *Science* **2014**, *345* (6198), 804–808. <https://doi.org/10.1126/science.1254910>.
- (65) Haumann, M.; Liebisch, P.; Müller, C.; Barra, M.; Grabolle, M.; Dau, H. Photosynthetic O_2 Formation Tracked by Time-Resolved x-Ray Experiments. *Science* **2005**, *310* (5750), 1019–1021. <https://doi.org/10.1126/science.1117551>.
- (66) Strickler, M. A.; Hillier, W.; Debus, R. J. No Evidence from FTIR Difference Spectroscopy That Glutamate-189 of the D1 Polypeptide Ligates a Mn Ion That Undergoes Oxidation during the S_0 to S_1 , S_1 to S_2 , or S_2 to S_3 Transitions in Photosystem II. *Biochemistry* **2006**, *45* (29), 8801–8811. <https://doi.org/10.1021/bi060583a>.
- (67) Clausen, J.; Winkler, S.; Hays, A. M.; Hundelt, M.; Debus, R. J.; Junge, W. Photosynthetic Water Oxidation in *Synechocystis* Sp. PCC6803: Mutations D1-E189K, R and Q Are without Influence on Electron Transfer at the Donor Side of Photosystem II. *Biochim. Biophys. Acta* **2001**, *1506* (3), 224–235. [https://doi.org/10.1016/S0005-2728\(01\)00217-1](https://doi.org/10.1016/S0005-2728(01)00217-1).
- (68) Suga, M.; Akita, F.; Sugahara, M.; Kubo, M.; Nakajima, Y.; Nakane, T.; Yamashita, K.; Umena, Y.; Nakabayashi, M.; Yamane, T.; et al. Light-Induced Structural Changes and the Site of O=O Bond Formation in PSII Caught by XFEL. *Nature* **2017**, *543* (7643), 131–135. <https://doi.org/10.1038/nature21400>.

- (69) Pantazis, D. A. Missing Pieces in the Puzzle of Biological Water Oxidation. *ACS Catal.* **2018**, *8* (10), 9477–9507. <https://doi.org/10.1021/acscatal.8b01928>.
- (70) Wang, J.; Askerka, M.; Brudvig, G. W.; Batista, V. S. Crystallographic Data Support the Carousel Mechanism of Water Supply to the Oxygen-Evolving Complex of Photosystem II. *ACS Energy Lett* **2017**, *2* (10), 2299–2306. <https://doi.org/10.1021/acsenergylett.7b00750>.
- (71) Amin, M.; Askerka, M.; Batista, V. S.; Brudvig, G. W.; Gunner, M. R. X-Ray Free Electron Laser Radiation Damage through the S-State Cycle of the Oxygen-Evolving Complex of Photosystem II. *J Phys Chem B* **2017**, *121* (40), 9382–9388. <https://doi.org/10.1021/acs.jpcc.7b08371>.
- (72) Amin, M.; Badawi, A.; Obayya, S. S. Radiation Damage in XFEL: Case Study from the Oxygen-Evolving Complex of Photosystem II. *Sci Rep* **2016**, *6*, 36492. <https://doi.org/10.1038/srep36492>.